ARTICLES
PUBLISHED ONLINE: 26 SEPTEMBER 2010 | DOI: 10.1038/NCHEM.838
nature chemistry

A bidentate Lewis acid with a telluronium ion as an anion-binding site

Haiyan Zhao and François P. Gabbaï*

The search for receptors that can selectively capture small and potentially toxic anions in protic media has sparked a renewed interest in the synthesis and anion-binding properties of polydentate Lewis acids. Seeking new paradigms to enhance the anion affinities of such systems, we synthesized a bidentate Lewis acid that contains a boryl and a telluronium moiety as Lewis acidic sites. Anion-complexation studies indicate that this telluronium borane displays a high affinity for fluoride in methanol. Structural and computational studies show that the unusual fluoride affinity of this bidentate telluronium borane can be correlated with the formation of a B–F → Te chelate motif supported by a strong lone-pair(F) → σ*(Te–C) donor–acceptor interaction. These results, which illustrate the viability of heavier chalcogenium centres as anion-binding sites, allow us to introduce a novel strategy for the design of polydentate Lewis acids with enhanced anion affinities.

The chemistry of polyfunctional Lewis acids is a rapidly expanding field with important applications in anion sensing. Most of the polyfunctional Lewis acids investigated to date contain group 12 (refs 1–4), 13 (refs 5–11) and 14 (refs 12–15) elements as Lewis acidic binding sites incorporated in both homonuclear[1–15] and heteronuclear[16–19] motifs[20]. Advances in the chemistry of boron-based heteronuclear bidentate Lewis acids show that anion binding at the boron centre can be assisted by the participation of a secondary Lewis acidic site[16–19]. Unlike most bidentate diboranes, some of these heteronuclear Lewis acids display an increased stability to protic media, as well as uncompromised anion affinities[18,19]. In a fundamental effort aimed at broadening the type of Lewis acidic moiety that could be employed in such systems, recently we became interested in the use of onium ions as secondary Lewis acidic sites. Initial results obtained in pursuit of this idea revealed that the latent Lewis acidity of phosphonium or sulfonium ions can be exploited for the recognition of potentially toxic anions such as fluoride and cyanide in protic environments[21,22]. These favourable effects can be illustrated by the anion affinity of the boron-based Lewis acids $[\mathbf{I}]^+$ and $[\mathbf{II}]^+$, which is enhanced by electron donation from a filled orbital of the anion (A^-) into a low-lying E–C σ^*-orbital of the onium centre in the corresponding complexes (Fig. 1).

These $A^- \rightarrow E^+$ donor–acceptor interactions are reminiscent of those involved in halogen-bonded (Type A)[23] or chalcogen-bonded (Type B)[24–29] complexes (Fig. 1). Although electron donation from the filled-orbital of the donor into the σ^*-orbital of the X–C or Ch–C bond (X = halogen, Ch = chalcogen) plays a role in the formation of such complexes, electrostatic effects that arise from the polarizability and relative electropositivity of the X or Ch atom may be the most important factor[23,27,30]. In agreement with this view, the strength of the donor–acceptor interactions observed in these complexes was shown to increase in the order Cl < Br < I for complexes of Type A (ref. 23) and S < Se < Te for complexes of Type B (ref. 27). Realizing that similar effects may control the strength of $A^- \rightarrow E^+$ donor–acceptor interactions, we are considering the use of heavier onium ions as Lewis acidic sites. In an initial exploration of this idea, we decided to synthesize and investigate a bidentate Lewis acid that contained a telluronium ion and compare its properties to those of its sulfur analogue. Although evidence for the Lewis acidity of telluronium ions can be gleaned from short anion–cation contacts in the crystal structures of their salts[31–34], efforts to use such onium ions for catalysis or anion recognition have not been reported previously.

Results

Implementing some of the synthetic approaches that we used recently for the synthesis of sulfonium boranes[22], the tetrakis(THF)lithium (THF = tetrahydrofuran) salt of dimesityl-1,8-naphthalenediylborate[35] was allowed to react with diphenylditelluride to afford the corresponding telluroborane (**1**, Fig. 2). The latter reacted smoothly with methyltriflate (MeOTf) to afford the borane–telluronium $[\mathbf{1}]^+$, which was isolated as the triflate salt (Fig. 2). For comparative purposes, we also synthesized the sulfonium analogue of [**1**]OTf, namely [**2**]OTf, by an analogous series of steps (Fig. 2). Compounds **1**, **2**, [**1**]OTf and [**2**]OTf were characterized by multinuclear nuclear magnetic resonance (NMR) spectroscopy and elemental analysis. In all four cases, the boron

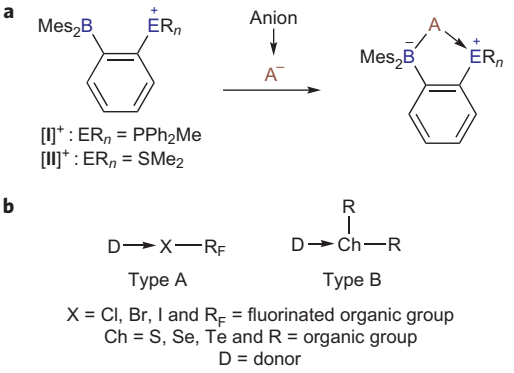

Figure 1 | Anion complexation by chelating cationic boranes and Lewis acidic properties of group 16 and 17 compounds. a, Anion chelation by *ortho*-phenylene-phosphonium and -sulfonium boranes. The boron-bound anion of the chelate complex interacts with the proximal onium centre through a donor–acceptor interaction (Me = methyl, Mes = mesityl, Ph = phenyl). **b**, Donor–acceptor interactions in halogen-bonded and chalcogen-bonded complexes.

Department of Chemistry, Texas A&M University, College Station, Texas 77843-3255, USA. *e-mail: francois@tamu.edu

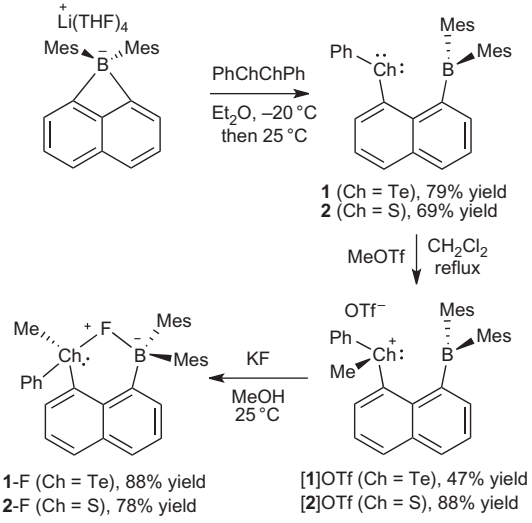

Figure 2 | Synthesis and reactivity of the chalcogenium borane salts [1]OTf and [2]OTf. Ring-opening of the tetrakis(THF)lithium salt of dimesityl-1,8-naphthalenediylborate with diphenyldichalcogenides in diethylether afforded the corresponding chalcogenoboranes **1** and **2**, which were converted into the chalcogenium borane triflate salts [**1**]OTf and [**2**]OTf by reaction with methyltriflate in dichloromethane. The latter were converted into the corresponding fluoride complexes **1**-F and **2**-F by reaction with KF in methanol.

centre remained trigonal planar, in agreement with the detection of a broad ^{11}B NMR resonance in the 60–70 parts per million (ppm) range[21,22]. For **1** and **2**, the ^{1}H NMR spectra exhibit six distinct resonances that correspond to the aromatic CH groups of the asymmetrically substituted naphthalene backbone. Four aryl (CH^{Mes}) and six methyl (CH_3^{Mes}) proton resonances were observed for the two mesityl (Mes) groups, which indicates the existence of a congested structure. The ^{1}H NMR spectra of [**1**]OTf and [**2**]OTf are consistent with the existence of two diastereomers that arise from chirality at the group 16 onium centre and helical chirality at the boron centre. Each of these diastereomers gives rise to four CH^{Mes} resonances and six CH_3^{Mes} resonances to give a total of eight CH^{Mes} and twelve CH_3^{Mes} signals. Accordingly, two resonances are observed for the group 16-bound methyl group. In the case of $[\mathbf{1}]^+$, the presence of these diastereomers can be ascertained further by the detection of two ^{125}Te NMR resonances at 660 and 677 ppm (refs 36,37), with an integration ratio that corresponds to those observed for the ^{1}H NMR signals of each diastereomer.

The crystal structures of **1** and **2** were determined experimentally (Fig. 3). The boron–chalcogen (B–Ch) distances in **1** (B–Te = 3.007(2) Å) and **2** (B–S = 2.952(3) Å) are well within the sum of the van der Waals radii of the two elements (1.50 Å for F, 1.80 Å for S and 2.10 Å for Te), which suggests the presence of a donor–acceptor interaction in these two compounds[38]. In agreement with this view, the boron atom in each compound adopts a slightly pyramidalysed structure, as shown by sum of the C–B–C angles (Σ(C–B–C) = 357.21(2)° for **1** and 358.3(2)° for **2**). This small angular distortion may also partly result from steric effects inherent to *peri*-substituted naphthalene derivatives. The existence of such effects is corroborated by the observation that the C(9)–C(1)–B angles in **1** (126.1(2)°) and **2** (126.9(2)°) deviate markedly from the ideal value of 120°. To shed further light on the bonding characteristics of **1** and **2**, the geometry of these two compounds was optimized using density functional theory (DFT) methods (functional: BP86; mixed basis set: Te: aug-cc-pvTz-pp; B: 6-31 + g(d′); S: 6-31 + g(d); C, H: 6-31g). The optimized geometries, which are close to those determined experimentally ($B–Te_{calc}$ = 3.014 Å and $B–S_{calc}$ = 2.971 Å) were subjected to a natural bond orbital (NBO) analysis, which identified a lone pair (lp)Ch → *p*(B) donor–acceptor interaction. As shown by deletion calculations[21], this interaction contributes to the stability of the molecules by E_{del} = 32.4 kcal mol^{-1} in the case of **1** and E_{del} = 16.5 kcal mol^{-1} in the case of **2** (Fig. 3). In turn, the boron centre of these derivatives experiences significant electron donation from the chalcogen. To assess the effect of group 16 methylation on this lp(Ch) → *p*(B) donor–acceptor interaction, the crystal structures of [**1**]OTf and [**2**]OTf were determined also (Fig. 3). Although there are no unusual intermolecular contacts in the structure of [**1**]OTf, one of the oxygen atoms of the triflate anion in [**2**]OTf forms a short contact of 2.904(5) Å with the tellurium centre, in agreement with the anticipated higher Lewis acidity of the telluronium unit. Further examination of these structures shows that:

(1) the boron atom in each cation becomes trigonal planar (Σ(C–B–C) = 359.8(5)° for [**1**]OTf and 359.7(2)° for [**2**]OTf);
(2) the B–Ch distance is increased significantly in the cationic species (B–Te = 3.244(6) Å for [**1**]OTf and B–S = 3.129(3) Å for [**2**]OTf).

These structural features may be assigned to the lower donicity induced by oxidative methylation of the group 16 element. The increased bulk around the chalcogen atom in [**1**]OTf and [**2**]OTf may also play a role in the increased B–Ch separation, a conclusion supported by the large C(9)–C(1)–B angles of 129.3(2)° and 129.4(5)° observed in [**1**]OTf and [**2**]OTf, respectively. Further insights into the strength of the lp(Ch) → *p*(B) donor–acceptor interaction in $[\mathbf{1}]^+$ and $[\mathbf{2}]^+$ were obtained from computational studies carried out at the level of theory used for **1** and **2**. The optimized structures of the two cations, which are close to those determined experimentally ($B–Te_{calc}$ = 3.222 Å and $B–S_{calc}$ = 3.091 Å), were subjected to NBO analyses. These analyses show that lp(Ch) → *p*(B) donor–acceptor interactions persist in $[\mathbf{1}]^+$ and $[\mathbf{2}]^+$. These interactions, which account for E_{del} = 10.8 kcal mol^{-1} and E_{del} = 8.2 kcal mol^{-1} and so for the stability of $[\mathbf{1}]^+$ and $[\mathbf{2}]^+$, are significantly lower than those in **1** and **2**, in agreement with the lower donicity of the chalcogenium groups (Fig. 3).

The ultraviolet–visible absorption spectra of these compounds in methanol (MeOH) display two distinct low-energy bands centred at 353 nm and 312 nm in the case of $[\mathbf{1}]^+$ and at 340 nm and 314 nm in case of $[\mathbf{2}]^+$ (Fig. 4). To elucidate the origin of these bands, the optimized structures of both cations were subjected to a time-dependent DFT (TD-DFT) calculation (functional: MPW1PW91; mixed basis set: Te: aug-cc-pvTz-pp; B: 6-31 + g(d′); S: 6-31 + g(d); C, H: 6-31g) using the polarizable continuum model solvation with methanol as a solvent. Examination of the simulated spectra indicates that each of the low-energy bands observed in the spectra of these cations mainly results from a few dominant excitations. The most red-shifted band at 353 nm for $[\mathbf{1}]^+$ and 340 nm for $[\mathbf{2}]^+$ arises from excitations (E_a and E_b, Fig. 4) that mostly involve the lowest unoccupied molecular orbital (LUMO) as the accepting orbital (Fig. 4). The second band at 312 nm for $[\mathbf{1}]^+$ and 314 nm for $[\mathbf{2}]^+$ involves excitations (E_c and E_d for $[\mathbf{1}]^+$; E_c, E_d and E_e for $[\mathbf{2}]^+$) in which LUMO + 1 acts as the main accepting orbital. Visualization of these orbitals indicates that the LUMOs of $[\mathbf{1}]^+$ and $[\mathbf{2}]^+$ carry an important contribution from the boron p_π-orbital (Fig. 4). This feature is reminiscent of simple triarylboranes, which usually display a low-energy band that results from electronic excitations from filled orbitals into the boron-centred LUMO[6,39–43]. Interestingly, the LUMO + 1 involved in the band detected at 312 nm for $[\mathbf{1}]^+$ and 314 nm for $[\mathbf{2}]^+$ bears an increased contribution from the Ch–C σ^*-orbital; this feature is especially noticeable in the case of the tellurium derivative $[\mathbf{1}]^+$ (Fig. 4). The localization of the LUMO and LUMO + 1

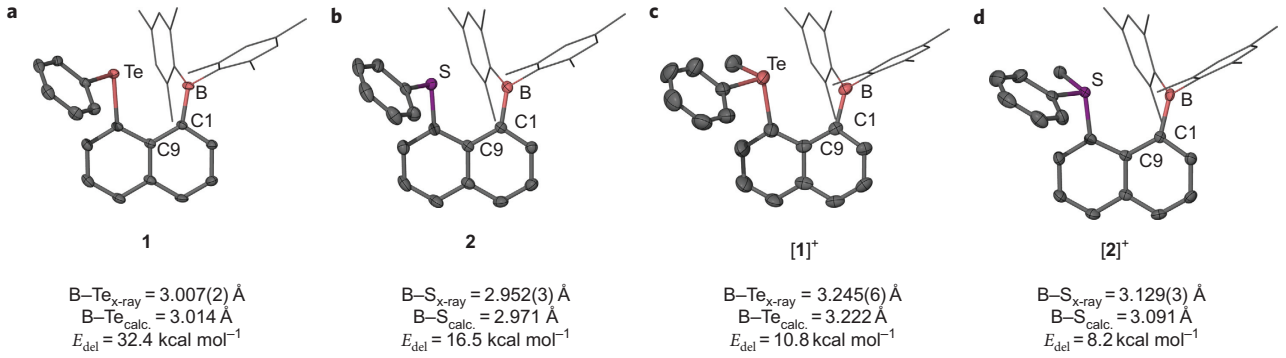

Figure 3 | Crystal structures of the chalcogenium borane salts and their neutral precursors. a–d, Ellipsoid drawings of **1** (**a**), **2** (**b**), [**1**]OTf (**c**) and [**2**]OTf (**d**) (thermal ellipsoids drawn at 50%; for clarity the hydrogen atoms are omitted, the mesityl ligands are represented by thin lines and the triflate anions are omitted). Only one diastereomer is shown for [**1**]OTf (**c**) and [**2**]OTf (**d**). For each compound, the crystallographically observed (B-Ch$_{X\text{-ray}}$) and DFT optimized (B-Ch$_{calc}$) boron–chalcogen separation is provided along with the deletion energy (E_{del}). The latter is obtained by zeroing the Kohn–Sham matrix elements that correspond to the lp(Ch) → p(B) interaction using the NBO program. E_{del} provides a comparative measure of the strength of the lp(Ch) → p(B) interaction present in these derivatives. (See Cambridge Crystallographic Data Centre (CCDC) 765274 (**1**), 765275 ([**1**]OTf), 765277 (**2**) and 765278 ([**2**]OTf)).

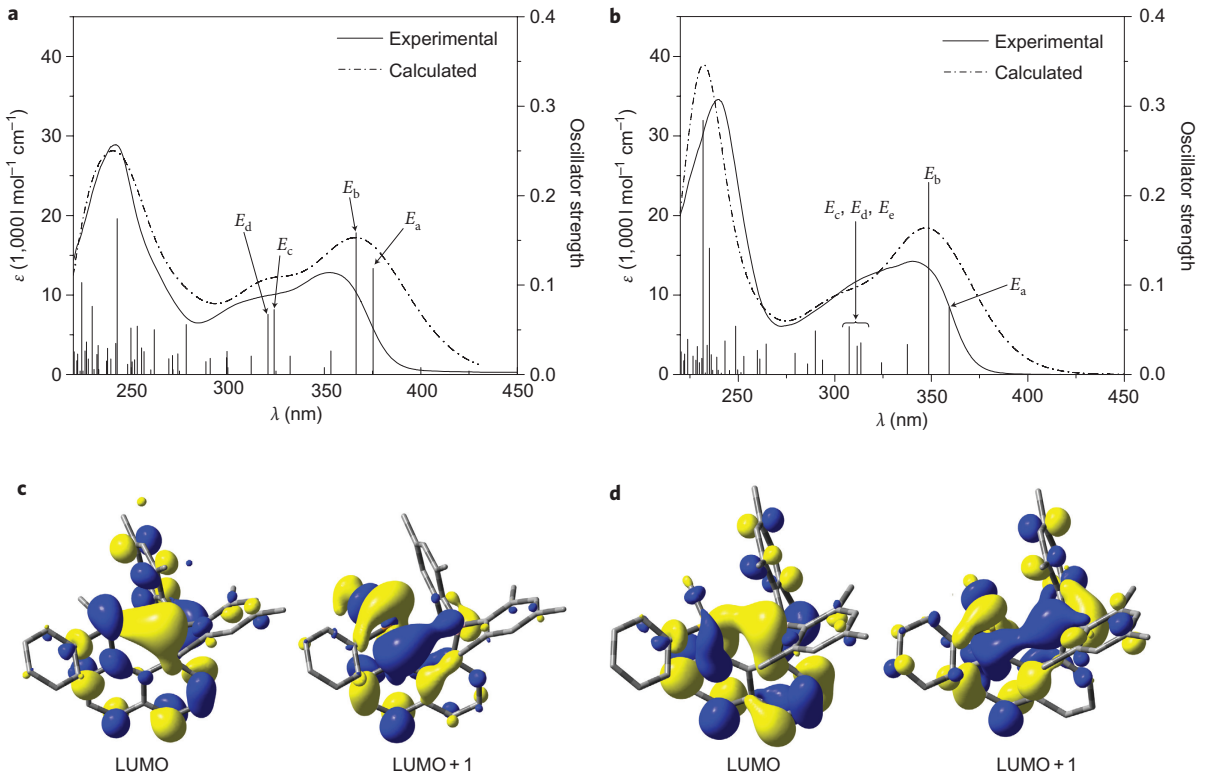

Figure 4 | Photophysical properties of the chalcogenium boranes [1]$^+$ and [2]$^+$. a,**b**, Experimental (methanol) and calculated ultraviolet–visible spectra for [**1**]$^+$ (**a**) and [**2**]$^+$ (**b**). The calculated spectra were obtained by TD-DFT calculations using the MPW1PW91 functional and a mixed basis set. In addition to the simulated spectra, the computed excitations are shown as thin lines with heights proportional to the calculated oscillator strengths. The excitations labelled as E_a–E_e are the main contributors to the low-energy absorption band observed in the spectra of these chalcogenium boranes. **c**,**d**, View of the LUMO and LUMO + 1 (isovalue = 0.03) of cations [**1**]$^+$ (**c**) and [**2**]$^+$ (**d**). These orbitals, which are implicated in $E_{a–e}$, bear a large component from the boron p_π-orbital and Ch–C σ^*-orbital.

orbitals on the neighbouring heteroelements, as well as their involvement in the low-energy electronic transitions, suggests that anion binding to these derivatives may be monitored very efficiently using spectrophotometric techniques[39]. It is also important that the localization of these two low-lying vacant orbitals on the two heteroelements bodes well for the occurrence of anion chelation.

With these two analogues in hand, we investigated their fluoride-ion affinity under dilute conditions in MeOH using ultraviolet–visible spectroscopy (Fig. 5). The addition of fluoride ions to [**1**]$^+$ (0.0673 mM) resulted in progressive quenching of the two lowest-energy bands, which suggests coordination of the fluoride anion to both the boron and tellurium atom. The resulting data was fitted

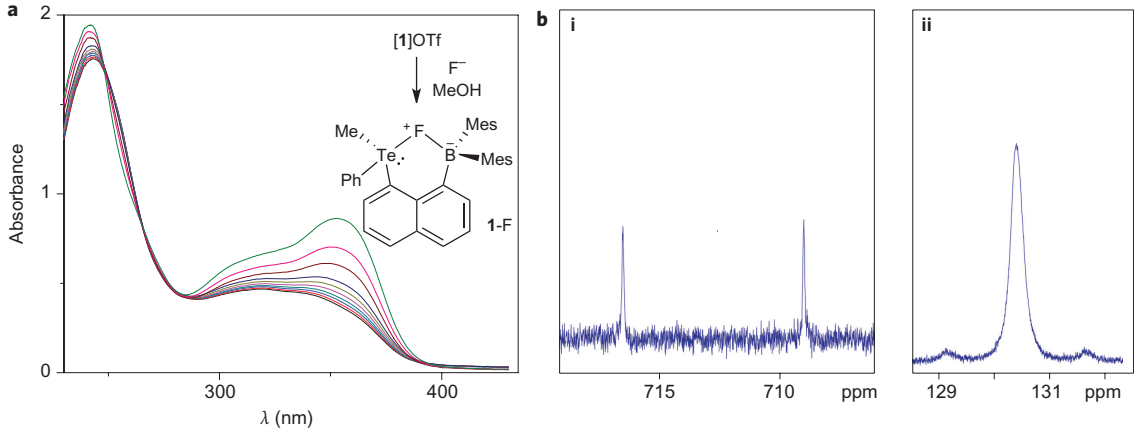

Figure 5 | Spectroscopic evidence for the formation and structure of 1-F. a, Changes observed in the ultraviolet–visible spectra of $[\mathbf{1}]^+$ (6.73×10^{-5} M) in MeOH on addition of a solution of fluoride anions. The observed quenching of the low-energy bands is consistent with the formation of **1**-F. Fitting the resulting data to a 1:1 binding isotherm affords a fluoride-binding constant K of 750 M^{-1}. **b**, ^{125}Te NMR (**i**) and ^{19}F NMR (**ii**) spectra of **1**-F. The presence of a doublet ($^1J_{Te-F} = 940$ Hz) in the ^{125}Te NMR spectrum indicates a strong interaction between the fluorine and tellurium nuclei. Accordingly, the ^{19}F NMR signal features two satellites that result from coupling to the ^{125}Te nucleus (7% natural abundance).

to a 1:1 binding isotherm to afford $K = 750$ (± 100) M^{-1} (Fig. 5). By contrast, the addition of 1,000 equivalents of fluoride ions to $[\mathbf{2}]^+$ did not result in any changes in the ultraviolet–visible spectrum, which indicates that $[\mathbf{2}]^+$ has no or very little affinity for fluoride ions in this solvent. A similar behaviour was observed for [1-Mes_2B-8-Me_2S-$C_{10}H_6$]$^+$, which also shows no marked affinity for fluoride ions in MeOH (ref. 22). Fluoride binding by $[\mathbf{1}]^+$ is also very selective, as indicated by the absence of any response observed on the addition of Cl^-, Br^-, I^-, OAc^-, NO_3^-, $H_2PO_4^-$ and HSO_4^- in MeOH.

In an effort to better understand the origin of the contrasting behaviour displayed by $[\mathbf{2}]^+$ and $[\mathbf{1}]^+$ towards fluoride anions, attempts to isolate **1**-F were undertaken (Fig. 2). Addition of fluoride to a MeOH solution of [**1**]OTf led to the rapid precipitation of **1**-F. The ^{11}B NMR resonance at 10.9 ppm is consistent with the presence of a four-coordinate boron centre. The ^{19}F NMR signal of **1**-F appears at −130.4 ppm. This chemical shift is unusual and appears to move significantly downfield when compared to shifts of other triarylfluoroborate species[39,44], such as o-$Mes_2FB(C_6H_4)NMe_3$ (−158.0 ppm), [1,2-(μ-F)-($(C_6F_5)_2B)_2C_6H_4$]$^-$ (−167.2 ppm) or [1-(Mes_2B)-(μ-F)-8-((C_6F_5)Hg)$C_{10}H_6$]$^-$ (−164.3 ppm)[18,45,46]. This downfield shift suggests that the fluoride anion in **1**-F is in an unusual chemical environment. In line with this argument, the ^{19}F resonance of **1**-F features two satellites, which indicates coupling to the ^{125}Te nucleus ($^1J_{Te-F} = 940$ Hz). This large ^{125}Te–^{19}F coupling is confirmed by the observation of a doublet ($\delta = 713$ ppm) split by 940 Hz in the ^{125}Te NMR spectrum. The magnitude of $^1J_{Te-F}$ in **1**-F is comparable to that observed in o-(C_6H_4-CH_2NMe_2)$_2TeF_2$ (969 Hz)[47]. Altogether, these spectroscopic features suggest that the fluorine atom is not only bound to the boron atom, but also forms a strong bond with the tellurium atom. Although no evidence for the formation of **2**-F was obtained in MeOH under dilute conditions, formation of this fluoride adduct could be driven by precipitation through the addition of an excess of KF to a MeOH solution of [**2**]OTf (Fig. 2). Some of its salient spectroscopic features include a ^{11}B NMR resonance at 8.7 ppm as well as a ^{19}F NMR signal at −150.7 ppm, in the range expected for typical triarylfluoroborate anions[39].

Compounds **1**-F and **2**-F were crystallized from dichloromethane. The crystal structures of these compounds (Fig. 6) clearly show that the:

(1) boron centre adopts a pyramidal geometry ($\Sigma_{(C-B-C)} = 339.5(1)^\circ$ for **2**-F and $343.0(3)^\circ$ for **1**-F);
(2) B–F bond length in **2**-F (1.481(2) Å) is slightly shorter than that in **1**-F (1.514(4) Å);
(3) F–Ch–C_{Ph} angle is close to linearity ($176.6(1)^\circ$ for **2**-F and $174.0(1)^\circ$ for **1**-F);
(4) S–F distance in **2**-F (2.548(1) Å) is slightly longer than the Te-F distance in **1**-F (2.506(2) Å), despite the larger size of the tellurium atom (Fig. 6).

Indeed, the Te–F bond distance in **1**-F is only moderately larger than the sum of the covalent radii of the two elements (1.95 Å)[48]. This Te–F bond distance can also be compared to those observed in other Te(IV) monofluoride species, such as [(μ-F)Te(CF_3)$_3$-dimethylformamide]$_\infty$ (ref. 49), a fluoride-bridged polymeric species connected by Te–F linkages of 2.138(2) Å and 2.566(2) Å. The overall coordination geometry of the tellurium atom in **1**-F is best described as a see-saw with a stereoactive lone pair perpendicular to the F–Te–C_{Ph} sequence.

To investigate the nature of the interaction between the group 16 element and the fluorine atom in **1**-F and **2**-F, we carried out an NBO analysis at the DFT-optimized structure (functional: BP86; mixed basis set: Te: aug-cc-pvTz-pp; B: 6-31 + g(d′); S: 6-31 + g(d); C, H: 6-31g). For both **1**-F and **2**-F, this analysis revealed the presence of two lp(F) → σ^*(Ch–C) donor–acceptor interactions. As depicted in Fig. 6, in the case **1**-F these two interactions involve two different fluorine lone-pair orbitals, which differ in their *s* and *p* character. The concomitant deletion of these two interactions leads to an increase of the total energy of the molecule by $E_{del} = 22.8$ kcal mol^{-1} for **1**-F and 9.2 kcal mol^{-1} for **2**-F, in line with the shorter Ch–F separation in **1**-F. The covalent component of the Ch–F interaction was probed further by performing an atom-in-molecule (AIM) analysis. This analysis shows that the value of the electron density at the bond critical point of the group 16-fluorine bond in **1**-F ($\rho(r) = 0.047$ e bohr^{-3}) is significantly larger than that in **2**-F ($\rho(r) = 0.035$ e bohr^{-3}), despite the increased diffuseness of the tellurium valence orbitals (Fig. 6). Altogether, these structural and computational results point to the higher Lewis acidity anticipated for the telluronium of $[\mathbf{1}]^+$ when compared to that of the sulfonium of $[\mathbf{2}]^+$. These observations, which are in line with previous studies on chalcogen-bonded species[27], can be correlated to the lower energy of the Ch–C σ^*-orbital in **1**-F, as well as to the greater electropositivity and polarizability of tellurium when compared to those of sulfur.

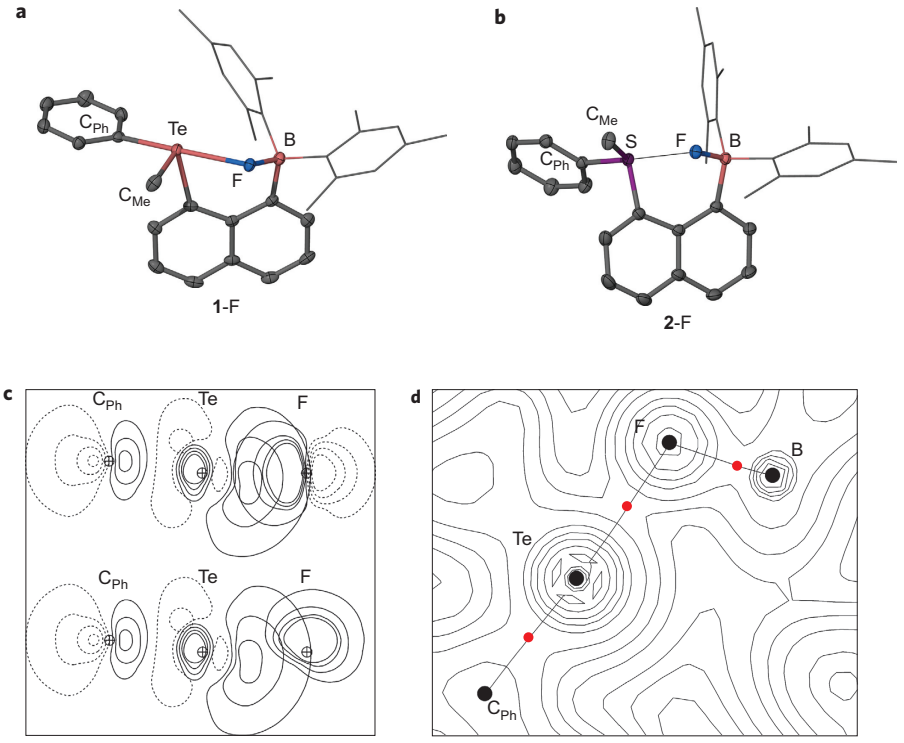

Figure 6 | Structural and bonding characteristics of 1-F and 2-F. a,**b**, Ellipsoid drawings of **1**-F (**a**) and **2**-F (**b**) (thermal ellipsoids drawn at 50%; for clarity the hydrogen atoms are omitted and the mesityl ligands are represented by thin lines). **c**, NBO contour plot that shows the two lp(F) → σ^*(Te–C) donor–acceptor interactions involved in **1**-F. The difference in hybridization of the two fluorine lone pairs involved in this interaction is evident from this view. **d**, AIM electron density map in the B–F–Te plane of **1**-F. The thin lines that connect the atoms represent the bond paths. For each bond path, the red dot indicates the position of the bond critical point. (See CCDC 765276 (**1**-F) and 765279 (**2**-F).)

Conclusion

The results presented in this article allow us to introduce a new strategy for the design of polyfunctional Lewis acids. This strategy, which is based on the use of heavier chalcogenium ions as Lewis acidic sites, takes advantage of the size, polarizability and electropositivity increases observed as the atom becomes larger. Although the increased polarizability and electropositivity of the tellurium atom in **1**-F lead to an enhancement of the ionic component of the group 16-anion interaction, its larger size allows for a reduction of intraligand repulsions, which makes interaction with the anionic guest more favourable. In turn, the anionic guest achieves a shorter approach to the tellurium atom, which leads to an increase of the covalent component of the chalcogen–anion interaction. Cumulatively, these effects make the telluronium centre of $[\mathbf{1}]^+$ a stronger Lewis acid than the sulfonium centre of $[\mathbf{2}]^+$, which thus provides a rationale for the enhanced fluoride affinity of $[\mathbf{1}]^+$. Although it was documented previously that heavier chalcogenium ions may act as acceptors[31–34], this property was not exploited in the context of molecular recognition. In turn, our work may lead to the development of novel Lewis acidic receptors or catalysts with telluronium ions as active sites.

Methods

Synthesis of 1. Diphenyl ditelluride (0.70 g, 1.71 mmol) was added to a suspension of tetrakis(THF)lithium dimesityl-1,8-naphthalenediylborate (1.00 g, 1.49 mmol) in diethyl ether (60 ml) at −20 °C. After stirring overnight at 25 °C, the reaction was quenched with water and extracted with dichloromethane (3 × 50 ml). The organic phases were combined, dried over $MgSO_4$ and filtered. The solvent was removed under vacuum to yield a yellow solid. The solid was washed with hexanes to afford compound **1** (0.68 g, yield 79%). A similar procedure was adopted for the synthesis of **2**. Characterization of **1**: ^{1}H NMR (400 MHz, $CDCl_3$) δ 0.82 (s, 3H), 1.80 (s, 3H), 2.22 (s, 3H), 2.26 (s, 3H), 2.32 (s, 3H), 2.38 (s, 3H), 6.50 (s, 1H, Mes-CH), 6.80 (s, 1H, Mes-CH), 6.85 (s, 1H, Mes-CH), 6.87 (s, 1H, Mes-CH), 7.04–7.19 (m, 5H, phenyl (ph)-CH), 7.33 (t, 1H, $^3J_{H-H}$ = 7.5 Hz, naphthyl (nap)-CH), 7.40–7.47 (m, 2H, nap-CH), 7.89 (d, 1H, J_{H-H} = 7.5 Hz, nap-CH), 7.93 (d, 1H, J_{H-H} = 7.8 Hz, nap-CH), 8.03 (d, 1H, J_{H-H} = 7.2 Hz, nap-CH); ^{13}C NMR (100 MHz, $CDCl_3$) δ 21.2, 22.9, 23.5, 25.5, 25.8, 120.5, 126.2, 126.6, 126.7, 127.2, 127.9, 128.9, 129.1, 129.7, 130.1, 130.2, 131.6, 133.8. 134.8, 135.1, 137.9, 139.8, 140.8, 141.3, 142.3, 143.4, 144.9; ^{11}B NMR (128 MHz, $CDCl_3$) δ + 60 (broad singlet (bs)); ^{125}Te NMR (126 MHz, $CDCl_3$) δ 646. Calculated for $C_{33}H_{34}BTe$: C, 70.40; H, 5.73; found: C, 70.38; H, 5.72.

Synthesis of [1]OTf. Methyl triflate (0.40 g, 2.44 mmol) was added to a solution of compound **1** (0.67 g, 1.16 mmol) in dichloromethane (25 ml) at 25 °C. The mixture was refluxed overnight and cooled to 25 °C. The solvent was removed under vacuum to yield a sticky yellow solid which was washed with diethyl ether to afford [**1**]OTf as a pale yellow solid (0.40 g, yield 47%). Single crystals of [**1**]OTf were obtained by slow evaporation of a dichloromethane solution. A similar procedure was adopted for the synthesis of [**2**]OTf. Characterization of [**1**]OTf: ^{1}H NMR (400 MHz, $CDCl_3$) major diastereomer (71%) δ 0.75 (s, 3H), 1.79 (s, 3H), 2.19 (s, 3H), 2.27 (s, 3H), 2.31 (s, 3H), 2.36 (s, 3H), 2.53 (s, 3H, S–CH_3), 6.60 (s, 1H, Mes-CH), 6.84 (s, 1H, Mes-CH), 6.97 (s, 1H, Mes-CH), 7.12 (s, 1H, Mes-CH), 7.14 (d, 1H, J_{H-H} = 7.6 Hz, nap-CH), 7.26–7.42 (m, 5H, ph-CH), 7.50–7.61 (m, 2H, nap-CH), 7.82 (t, 1H, J_{H-H} = 8.0 Hz, nap-CH), 8.07–8.13 (m, 2H, nap-CH); minor diastereomer (29%) δ 0.79 (s, 3H), 1.68 (s, 3H), 1.91 (s, 3H), 2.22 (s, 3H), 2.35 (s, 3H), 2.57 (s, 3H), 2.68 (s, 3H, S–CH_3), 6.43 (s, 1H, Mes-CH), 6.46 (s, 1H, Mes-CH), 6.79 (s, 1H, Mes-CH), 7.00 (s, 1H, Mes-CH), 7.26–7.42 (m, 5H, ph-CH), 7.50–7.67 (m, 5H, nap-CH), 8.21 (d, 1H, J_{H-H} = 7.6 Hz, nap-CH); ^{13}C NMR (100 MHz, $CDCl_3$) major diastereomer δ 11.9, 21.2, 21.3, 22.6, 22.7, 25.0, 25.1; minor diastereomer δ 20.9, 21.0, 22.6, 22.7, 24.7, 24.7, 24.9. Remaining peaks for both diastereomers δ 118.7, 120.6, 121.9, 124.4, 124.9, 125.2, 126.9, 127.5, 127.7, 127.9, 128.1, 128.3, 129.4, 129.5, 129.7, 129.9, 130.3, 130.5, 130.7, 131.0, 131.1, 131.6, 131.6, 131.9, 132.3, 132.6, 133.2, 133.3, 134.0, 134.2, 134.4, 134.5, 134.6, 136.8, 137.7, 138.9, 139.0, 139.7, 139.7, 139.8, 139.9, 140.1, 140.5, 140.8, 141.2, 141.7, 142.1, 142.8, 143.2, 145.9, 147.0; ^{125}Te NMR (126 MHz, $CDCl_3$) δ 660, 677. Calculated for $C_{36}H_{36}BO_3F_3STe$: C, 58.11; H, 4.88; found: C, 57.96; H, 4.88.

Synthesis of 1-F. [**1**]OTf (0.048 g, 0.074 mmol) was dissolved in a saturated KF methanol solution which gave a white precipitate. After 15 minutes, this precipitate was isolated by filtration and dried under vacuum to afford **1**-F (0.035 g, yield 88%). Single crystals of **1**-F were obtained by slow evaporation of a chloroform solution. A similar procedure was adopted for the synthesis of **2**-F. Characterization of **1**-F: ^{1}H NMR (400 MHz, $CDCl_3$) δ 1.69 (s, 3H), 1.93 (d, 3H, J_{H-F} = 7.2 Hz), 2.02 (s, 3H),

2.14 (s, 3H), 2.21 (s, 3H), 2.27 (s, 3H), 2.72 (dd, 3H, $J_{H-F} = 2.4$ Hz $J_{H-Te} = 16.3$ Hz), 6.60 (s, 1H, Mes-CH), 6.72 (s, 2H, Mes-CH), 6.75 (s, 1H, Mes-CH), 7.15 (t, 1H, $J_{H-H} = 7.6$ Hz, nap-CH), 7.27 (d, 1H, $J_{H-H} = 8.4$ Hz, nap-CH), 7.36 (t, 1H, $J_{H-H} = 7.6$ Hz, nap-CH), 7.46–7.53 (m, 5H, ph-CH), 7.64 (d, 1H, $J_{H-H} = 7.6$ Hz, nap-CH), 7.70 (d, 1H, $J_{H-H} = 6.8$ Hz, nap-CH), 7.94 (d, 1H, $J_{H-H} = 8.0$ Hz, nap-CH); ^{13}C NMR (100 MHz, $CDCl_3$) δ 13.06 (d, Te–CH_3, $J_{C-F} = 11$ Hz), 20.9, 21.0, 24.2 (d, Mes-CH_3, $J_{C-F} = 7.3$ Hz), 24.3, 24.8, 25.6, 123.7, 123.9, 126.7, 127.1, 127.8, 128.6, 129.1, 129.7, 129.9, 130.1, 130.5, 131.3, 132.9, 133.2, 134.8, 134.8, 135.3, 136.5, 136.5, 139.0, 141.0, 141.0, 142.1, 142.2, 142.3, 144.6; ^{11}B NMR (128 MHz, d_6-acetone) δ + 10.9 (bs); ^{19}F NMR (375.9 MHz, $CDCl_3$) δ − 130.4 (d, $J_{Te-F} = 940$ Hz); ^{125}Te NMR (126 MHz, $CDCl_3$) δ 713 (d, $J_{Te-F} = 940$ Hz). Calculated for $C_{35}H_{36}BFTe$: C, 68.46; H, 5.91; found: C, 68.66; H, 5.94.

Fluoride ion-binding studies. A solution of [**1**]OTf (3 ml, 6.73×10^{-5} M, methanol) was placed in the cuvette and titrated with incremental amounts of fluoride anions by the addition of a solution of KF in MeOH (0.3159 M). The absorbance was monitored at $\lambda = 353$ nm ($\varepsilon = 12{,}800$ for [**1**]OTf and $\varepsilon = 3{,}750$ for **1**-F). The experimental data obtained were fitted to a 1:1 binding isotherm, which indicated that the fluoride binding constant of [**1**]OTf is equal to 750 ($\pm$100) M^{-1} in MeOH.

Received 11 February 2010; accepted 12 August 2010; published online 26 September 2010

References

1. Wuest, J. D. Multiple coordination and activation of Lewis bases by multidentate Lewis acids. *Acc. Chem. Res.* **32,** 81–89 (1999).
2. Wedge, T. J. & Hawthorne, M. F. Multidentate carborane-containing Lewis acids and their chemistry: mercuracarborands. *Coord. Chem. Rev.* **240,** 111–128 (2003).
3. Shur, V. B. & Tikhonova, I. A. Perfluorinated polymercuramacrocycles as anticrowns. Applications in catalysis. *Russ. Chem. Bull.* **52,** 2539–2554 (2003).
4. Taylor, T. J., Burress, C. N. & Gabbaï, F. P. Lewis acidic behavior of fluorinated organomercurials. *Organometallics* **26,** 5252–5263 (2007).
5. Kilyanek, S. M., Fang, X. & Jordan, R. F. Synthesis and reactivity of a tetragallium macrocycle. *Organometallics* **28,** 300–305 (2009).
6. Hudnall, T. W., Chiu, C.-W. & Gabbaï, F. P. Fluoride ion recognition by chelating and cationic boranes. *Acc. Chem. Res.* **42,** 388–397 (2009).
7. Piers, W. E. The chemistry of perfluoroaryl boranes. *Adv. Organomet. Chem.* **52,** 1–76 (2005).
8. Melaïmi, M. & Gabbaï, F. P. Bidentate group 13 Lewis acids with *ortho*-phenylene and *peri*-naphthalenediyl backbones. *Adv. Organomet. Chem.* **53,** 61–99 (2005).
9. Emslie, D. J. H., Piers, W. E. & Parvez, M. 2,2′-diborabiphenyl: a Lewis acid analogue of 2,2′-bipyridine. *Angew. Chem. Int. Ed.* **42,** 1252–1255 (2003).
10. Katz, H. E. Recent advances in multidentate anion complexation. *Inclusion Compd* **4,** 391–405 (1991).
11. Uhl, W. & Hannemann, F. A methylene bridged dialuminum compound as a chelating Lewis acid-complexation of azide and acetate anions by $R_2Al–CH_2–AlR_2$ [R=CH($SiMe_3$)$_2$]. *J. Organomet. Chem.* **579,** 18–23 (1999).
12. Tagne Kuate, A. C., Reeske, G., Schurmann, M., Costisella, B. & Jurkschat, K. Organotin compounds Ph_2XSnCH_2-[19]-crown-6 (X = Ph, F, Cl, Br, I, SCN) and $Ph_2ISnCH_2Sn(I)PhCH_2$-[19]-crown-6 as ditopic receptors for potassium salts. *Organometallics* **27,** 5577–5587 (2008).
13. Zobel, B., Duthie, A., Dakternieks, D. & Tiekink, E. R. T. α,ω-Bis(trichlorostannyl)alkanes as bis(monodentate) Lewis acids toward halide ions. *Organometallics* **20,** 3347–3350 (2001).
14. Tamao, K., Hayashi, T., Ito, Y. & Shiro, M. Pentacoordinate anionic bis(siliconates) containing a fluorine bridge between two silicon atoms. Synthesis, solid-state structures, and dynamic behavior in solution. *Organometallics* **11,** 2099–2114 (1992).
15. Newcomb, M., Horner, J. H., Blanda, M. T. & Squattrito, P. J. Macrocycles containing tin. Solid complexes of anions encrypted in macrobicyclic Lewis acidic hosts. *J. Am. Chem. Soc.* **111,** 6294–6301 (1989).
16. Kawachi, A., Tani, A., Shimada, J. & Yamamoto, Y. Synthesis of B/Si bidentate Lewis acids, *o*-(fluorosilyl)(dimesitylboryl)benzenes, and their fluoride ion affinity. *J. Am. Chem. Soc.* **130,** 4222–4223 (2008).
17. Boshra, R. *et al.* Simultaneous fluoride binding to ferrocene-based heteronuclear bidentate Lewis acids. *Inorg. Chem.* **46,** 10174–10186 (2007).
18. Melaïmi, M. & Gabbaï, F. P. A heteronuclear bidentate Lewis acid as a phosphorescent fluoride sensor. *J. Am. Chem. Soc.* **127,** 9680–9681 (2005).
19. Lee, M. H. & Gabbaï, F. P. Synthesis and properties of a cationic bidentate Lewis acid. *Inorg. Chem.* **46,** 8132–8138 (2007).
20. Wade, C. R., Broomsgrove, A. E. J., Aldridge, S. & Gabbaï, F. P. Fluoride ion complexation and sensing using organoboron compounds. *Chem. Rev.* **110,** 3958–3984 (2010).
21. Hudnall, T. W., Kim, Y.-M., Bebbington, M. W. P., Bourissou, D. & Gabbaï, F. P. Fluoride ion chelation by a bidentate phosphonium/borane Lewis acid. *J. Am. Chem. Soc.* **130,** 10890–10891 (2008).
22. Kim, Y., Zhao, H. & Gabbaï, F. P. Sulfonium boranes for the selective capture of cyanide ions in water. *Angew. Chem. Int. Ed.* **48,** 4957–4960 (2009).
23. Metrangolo, P. & Resnati, G. Halogen bonding: a paradigm in supramolecular chemistry. *Chem. Eur. J.* **7,** 2511–2519 (2001).
24. Sudha, N. & Singh, H. B. Intramolecular coordination in tellurium chemistry. *Coord. Chem. Rev.* **135,** 469–515 (1994).
25. Burling, F. T. & Goldstein, B. M. Computational studies of nonbonded sulfur–oxygen and selenium–oxygen interactions in the thiazole and selenazole nucleosides. *J. Am. Chem. Soc.* **114,** 2313–2320 (1992).
26. Gleiter, R., Werz, D. B. & Rausch, B. J. A world beyond hydrogen bonds? Chalcogen–chalcogen interactions yielding tubular structures. *Chem. Eur. J.* **9,** 2676–2683 (2003).
27. Bleiholder, C., Werz, D. B., Köppel, H. & Gleiter, R. Theoretical investigations on chalcogen–chalcogen interactions: what makes these nonbonded interactions bonding? *J. Am. Chem. Soc.* **128,** 2666–2674 (2006).
28. Tripathi Santosh, K. *et al. o*-Hydroxylmethylphenylchalcogens: synthesis, intramolecular nonbonded chalcogen $\cdots$ OH interactions, and glutathione peroxidase-like activity. *J. Org. Chem.* **70,** 9237–9247 (2005).
29. Hayashi, S. & Nakanishi, W. Noncovalent Z $\cdots$ Z (Z=O, S, Se, and Te) interactions: how do they operate to control fine structures of 1,8-dichalcogene-substituted naphthalenes? *Bull. Chem. Soc. Jpn* **81,** 1605–1615 (2008).
30. Lommerse, J. P. M., Stone, A. J., Taylor, R. & Allen, F. H. The nature and geometry of intermolecular interactions between halogens and oxygen or nitrogen. *J. Am. Chem. Soc.* **118,** 3108–3116 (1996).
31. Chandrasekhar, V. & Thirumoorthi, R. Halide-capped tellurium-containing macrocycles. *Inorg. Chem.* **48,** 10330–10337 (2009).
32. Klapötke, T. M., Krumm, B. & Scherr, M. Synthesis and structures of triorganochalcogenium (Te, Se, S) dinitramides. *Eur. J. Inorg. Chem.* 4413–4419 (2008).
33. Naumann, D., Tyrra, W., Hermannn, R., Pantenburg, I. & Wickleder, M. S. Syntheses and properties of tetrakis(pentafluorophenyl)tellurium, $Te(C_6F_5)_4$, and related compounds – single crystal structures of tris(pentafluorophenyl)tellurium bromide, $Te(C_6F_5)_3Br$, tris(pentafluorophenyl)tellurium trifluoromethanesulfonate, $[Te(C_6F_5)_3][OSO_2CF_3]$, and bis(pentafluorophenyl) tellurium oxide, $Te(C_6F_5)_2O$. *Z. Anorg. Allg. Chem.* **628,** 833–842 (2002).
34. Sato, S., Kondo, N., Horn, E. & Furukawa, N. Monooxytellurane(IV) derivatives ([10-Te-4-(C3O)]). Syntheses and molecular structure of triaryltelluronium carboxylate compounds. *Organometallics* **17,** 1897–1900 (1998).
35. Hoefelmeyer, J. D. & Gabbaï, F. P. Synthesis of 1,8-diborylnaphthalenes by the ring-opening reaction of a new anionic boron-bridged naphthalene derivative. *Organometallics* **21,** 982–985 (2002).
36. Laali, K., Chen, H. Y. & Gerzina, R. J. Selenium-77, tellurium-125, and carbon-13 NMR chemical shifts and one-bond $^{77}Se–^{13}C$, $^{125}Te–^{13}C$, and $^{13}C–^{1}H$ coupling constants of trialkylselenonium and -telluronium triflates, protonated dialkylselenonium and -telluronium cations, and their corresponding donor–acceptor complexes. *J. Org. Chem.* **52,** 4126–4128 (1987).
37. Saito, S., Zhang, J., Tanida, K., Takahashi, S. & Koizumi, T. A systematic ^{125}Te NMR study of organotellurium compounds: the effect of oxidation states and substituents. *Tetrahedron* **55,** 2545–2552 (1999).
38. Batsanov, S. S. Van der waals radii of elements. *Inorg. Mater.* **37,** 871–885 (2001).
39. Yamaguchi, S., Akiyama, S. & Tamao, K. Colorimetric fluoride ion sensing by boron-containing π-electron systems. *J. Am. Chem. Soc.* **123,** 11372–11375 (2001).
40. Entwistle, C. D. & Marder, T. B. Boron chemistry lights the way: optical properties of molecular and polymeric systems. *Angew. Chem. Int. Ed.* **41,** 2927–2931 (2002).
41. Yamaguchi, S. & Wakamiya, A. Boron as a key component for new π-electron materials. *Pure Appl. Chem.* **78,** 1413–1424 (2006).
42. Parab, K., Venkatasubbaiah, K. & Jäkle, F. Luminescent triarylborane-functionalized polystyrene: synthesis, photophysical characterization, and anion-binding studies. *J. Am. Chem. Soc.* **128,** 12879–12885 (2006).
43. Hudson, Z. M. & Wang, S. Impact of donor–acceptor geometry and metal chelation on photophysical properties and applications of triarylboranes. *Acc. Chem. Res.* **42,** 1584–1596 (2009).
44. Lee, M. H., Agou, T., Kobayashi, J., Kawashima, T. & Gabbaï, F. P. Fluoride ion complexation by a cationic borane in aqueous solution. *Chem. Commun.* 1133–1135 (2007).
45. Hudnall, T. W. & Gabbaï, F. P. Ammonium boranes for the selective complexation of cyanide or fluoride ions in water. *J. Am. Chem. Soc.* **129,** 11978–11986 (2007).
46. Williams, V. C. *et al.* New bifunctional perfluoroaryl boranes. Synthesis and reactivity of the *ortho*-phenylene-bridged diboranes 1,2-$[B(C_6F_5)_2]_2C_6X_4$ (X = H, F). *J. Am. Chem. Soc.* **121,** 3244–3245 (1999).
47. Hammerl, A., Klapötke, T. M., Krumm, B. & Scherr, M. Tellurium(IV) fluorides and azides containing the nitrogen donor substituent R = 2-$Me_2NCH_2C_6H_4$;

crystal structure of $RTeF_3$ and of an unusual tellurium(VI) fluoride salt. *Z. Anorg. Allg. Chem.* **633,** 1618–1626 (2007).
48. Cordero, B. *et al*. Covalent radii revisited. *Dalton Trans.* 2832–2838 (2008).
49. Kirij, N. V., Yagupolskii, Y. L., Tyrra, W., Pantenburg, I. & Naumann, D. The structure of tris(trifluoromethyl)tellurium fluoride dimethylformamide, $[Te(CF_3)_3$-DMF(μ-F)]. *Z. Anorg. Allg. Chem.* **633,** 943–945 (2007).

Acknowledgements

This work was supported by the National Science Foundation (CHE-0952912) and the Welch Foundation (A-1423).

Author contributions

H.Z. carried out all of the experimental, analytical and computational work. F.P.G. directed the project and assisted with the preparation of the manuscript.

Additional information

The authors declare no competing financial interests. Supplementary information and chemical compound information accompany this paper at www.nature.com/naturechemistry. Reprints and permission information is available online at http://npg.nature.com/reprintsandpermissions/. Correspondence and requests for materials should be addressed to F.P.G.